

APPLICATION OF THE 3D CRS WORKFLOW IN A CRYSTALLINE ROCK ENVIRONMENT

K. A. Ahmed, B. Schwarz, and D. Gajewski

email: *khawar-ashfaq.ahmed@uni-hamburg.de*

keywords: *3D CRS, Hard rock*

ABSTRACT

Seismic data from crystalline or hard rock environments usually exhibit a poor signal-to-noise (S/N) ratio due to low acoustic impedances in the subsurface. Moreover, instead of continuous reflections we observe a lot of steeply dipping events resembling parts of diffractions. The conventional seismic processing (CMP stack and DMO) is not ideally suited for imaging such type of data. Common-reflection-surface (CRS) processing considers more traces during the stack than CMP processing and the resulting image displays a better quality. In the last decade, the CRS method was established as a powerful tool to provide improved images, especially for low fold or low S/N data. The CRS stack and all attributes linked to it are obtained using a coherence based automatic data-driven optimization procedure. The CRS workflow was applied to the 3D Schneeberg crystalline rock seismic data which were acquired for geothermal exploration. The CRS stack itself provided an image of improved S/N-ratio but the quality was not suitable for interpretation. For data from environments with low acoustic impedance and poor velocity information the coherence automatically obtained in the optimization procedure provides an alternative way to image the subsurface. For this data the coherency image provided the best results for an initial analysis. Because of the large number of diffractions in the data leading to numerous conflicting dips and crossing image patterns, stacks are difficult to interpret. Time-migrated data helped to identify several major fault structures, which coincide with geological features of the considered area. The distribution of diffraction apices in the time-migrated section shows a distinct high where several fracture systems intersect. If these diffractions are the response of open fractures the area could serve as a natural heat exchanger to generate geothermal energy.

INTRODUCTION

3D seismic imaging is a challenge for data acquired in hard rock environments. The reason for this is the small reflectivity/acoustic impedance and S/N ratio compared to data from sedimentary basins (see, e.g., Milkereit et al., 2000; Malehmir et al., 2012). Contrary to typical reflection data where we observe continuous events over large lateral distances hard rock data are usually dominated by diffractions or parts of diffraction events which leads to a criss-cross pattern and numerous conflicting dip features in the stacked sections. This challenges any kind of geological interpretation. Because of the small lateral extend of events in hard rock data, velocity determination is difficult, Moreover, the velocity in hard rock is usually high and the resulting moveouts are small which provides an additional challenge in the data processing. These problems in velocity analysis influence the quality of the stacked data and may lead to an unsatisfactory image not very suitable for geological interpretation.

It was demonstrated previously that the common-reflection-surface (CRS) stacking method has advantages for low fold and/or low signal-to-noise (S/N) data when compared with CMP stacking (Hertweck et al., 2007; Baykulov et al., 2011). This observation suggests to apply the CRS method to hard rock data. It is an important feature that the fold in CRS processing is considerably higher than

the fold in CMP processing which helps to image weak events and to improve the S/N-ratio of the stacked section. The CRS method (Mann et al., 1999; Bergler et al., 2002) is an automatic entirely data driven approach. It provides next to the stack itself several kinematic wavefield attributes and the corresponding coherence for each sample in the stacked data volume. The wavefield attributes have many applications in CRS processing like multiple suppression (Dümmong and Gajewski, 2008), NIP-wave tomography (Duveneck, 2004), diffraction processing and imaging (Dell and Gajewski, 2011), pre-stack data enhancement, data interpolation and regularization (Baykulov and Gajewski, 2009) just to name a few.

In a joint project with the Leibniz Institute for Applied Geophysics, Hannover, Germany and the University of Freiberg, Freiberg, Germany a 3D reflection seismic experiment was conducted in the area of the city of Schneeberg, Saxony, Germany. The field work is part of a pre-site survey for a geothermal exploration project. The subsurface in this area is complex and dominated by steep faulting in the crystalline rocks. The data show a lot of scattering due to the fractured zones and hydrothermal veins. The processing of this type of seismic data is a challenge because of the above mentioned reasons. Conventional CMP-DMO-based processing did not provide satisfactory results. Therefore, 3D CRS processing was applied here to achieve a better S/N ratio and to obtain an interpretable stacked volume.

In the next section of the paper we briefly discuss the foundations of the 3D CRS method before we introduce the area of investigation in some more detail. The application of the CRS method to 3D data is then discussed in the following sections. The data-driven automatic CRS approach delivers stacked sections and several volumes of wavefield attributes which provide a first image of the subsurface. Time-migrated coherency sections provide images best suitable for interpretation. A brief discussion of the major geological features and some conclusions finalize the paper.

BASICS OF THE 3D-CRS WORKFLOW

The CRS stack (Mann et al., 1999) was originally developed to obtain simulated zero-offset (ZO) sections or volumes from seismic multi-coverage data. The method is based on a stacking operator that is of second order in the midpoint and half-offset coordinates x_m and h , i.e., it is of hyperbolic shape. The CRS stacking operator at a given zero-offset location (x_0, t_0) is determined by a number of parameters related to the coefficients of the second order travel time expansion. For each zero-offset sample to be simulated, the optimum stacking operator is found by varying these parameter values within predefined boundaries. These parameters or attributes define the shape of the operator. Performing a coherence analysis in the pre-stack domain provides the attributes with the best fit to the data. The parameters which yield the highest coherence value describe the optimum stacking operator.

3D common-reflection-surface stack

In the 3D case (Bergler et al., 2002; Müller, 2003), the traveltimes surface is formulated in terms of the two symmetric 2×2 curvature matrices \mathbf{M}_{nip} and \mathbf{M}_n respectively and the two-component slope vector \mathbf{p}_m , leading to an eight parameter expression:

$$t^2(\Delta\mathbf{x}_m, h) = (t_0 + \mathbf{p}_m \Delta\mathbf{x}_m)^2 + 2t_0 \left(\Delta\mathbf{x}_m^T \mathbf{M}_n \Delta\mathbf{x}_m + \mathbf{h}^T \mathbf{M}_{nip} \mathbf{h} \right) \quad (1)$$

Because the CRS operator can be derived by a Taylor expansion in midpoint and half-offset coordinates these stacking parameters represent first and second order traveltimes derivatives with respect to midpoint and half-offset coordinates. As long as the processing stays in time, no physical interpretation of the parameters is required. The CRS method and the stacking parameter estimation is an entirely data-driven fitting approach where the optimization of the operator is performed with the coherence as objective function. The coherence measure used is the semblance.

For the use of the attributes in processing and imaging a physical interpretation is available. If a locally constant near-surface velocity v_0 is known, the CRS operator can be written in a form which allows the interpretation of the stacking parameters as attributes describing two hypothetical emerging wave fronts at the considered surface location x_0 . These are the so-called normal-incidence point (NIP) wave and the normal (N) wave (Hubral, 1983). The NIP wave would be observed at x_0 if a point-source were placed at

the NIP of the zero-offset ray on the reflector in the subsurface, while the N wave would be obtained if an exploding reflector element -the CRS- were placed around the NIP in the subsurface. Because of the link to wavefront curvatures the stacking parameters are also called kinematic wavefield attributes. We will use both terms synonymously. The relation of the stacking parameters to the kinematic wavefield attributes is given by the following relations:

$$\mathbf{p}_m = \frac{1}{v_0} (\cos \alpha \sin \beta, \sin \alpha \cos \beta)^T \quad (2)$$

$$\mathbf{M}_{nip} = \frac{1}{v_0} \mathbf{H} \mathbf{K}_{nip} \mathbf{H}^T \quad (3)$$

$$\mathbf{M}_n = \frac{1}{v_0} \mathbf{H} \mathbf{K}_n \mathbf{H}^T \quad (4)$$

where α is azimuth, β is dip angle and \mathbf{H} is the 2×2 upper left sub matrix of the 3×3 transformation matrix from the wavefront coordinate system into the registration surface. The 3D CRS stack is just one product of the method. Next to the simulated ZO section and a number of volumes containing the optimum kinematic wavefield attributes, the maximum coherence for each ZO sample is obtained. After this brief introduction of the 3D CRS method and the kinematic wavefield attributes we discuss now the basic features of the study area.

AREA OF STUDY

Schneeberg is a town in the state of Saxony, Germany (Figure 1), located close to the border of the Czech Republic. Next to the surface geology, (Figure 2) also in-line and cross-line coordinates of the 3D survey are displayed. These coordinates are used in the following to describe the location of vertical sections or specific locations out of the 3D volume.

The structure and tectonics of the study area include a massive granitic igneous body overlapping with a number of low, medium and high grade metamorphic rock units. There are also patches of the sedimentary environments in the vicinity of this area. The origin of the igneous body goes back to an important Cambro-Ordovician phase of rifting, which is detectable almost everywhere in Europe (Emmermann and Wohlenberg, 1988). The alternating metamorphic blocks are on top of the igneous body in an inclined position derived from areas south of the Saxothuringian Zone. This massive igneous body is the prominent feature in this area which has high reflectivity at the transition zone between the metamorphic and igneous rocks and exhibits high velocities.

There is a major steep dipping fault system called *Roter Kamm* which runs through the igneous body (Figure 3). Some conjugate faulting can be observed in the upper area in NE which runs till the Roter Kamm crossing it perpendicularly and cutting this structure in SW direction. This area is highly fractured with steep dipping tectonics. At the surface the Roter Kamm is characterized by fault systems representing a major structure separating two different types of zones. The dip of the fault and the overlying rocks of the igneous body is towards north-east. It is assumed that the Roter Kamm will form also a prominent feature in the seismic cubes. In the next section we describe the application of the CRS method to the Schneeberg data.

CRS APPLICATION

The 3D CRS processing was applied to the Schneeberg crystalline rock reflection data. The data have a very poor signal-to-noise ratio typical for hard rock environments. Figure 4a shows the image of the automatic CMP stack for cross-line 600. The automatic stack is part of the procedure to determine CRS attributes (Mann et al., 1999; Müller, 2003) and represents the coherency-based determination of the CMP stacking velocity for each ZO sample. It can be described as an automatic data-driven way of velocity analysis. As expected, the image quality is very poor due to a low S/N ratio of the data. To stack energy with an analytic operator in complex media like hard rock is difficult. Differences in phase due to an imperfect fit of the operator decrease the stack amplitude. A geological interpretation based on the automatic CMP stack appears to be a big challenge.



Figure 1: Geographical map of Germany with the study area marked.

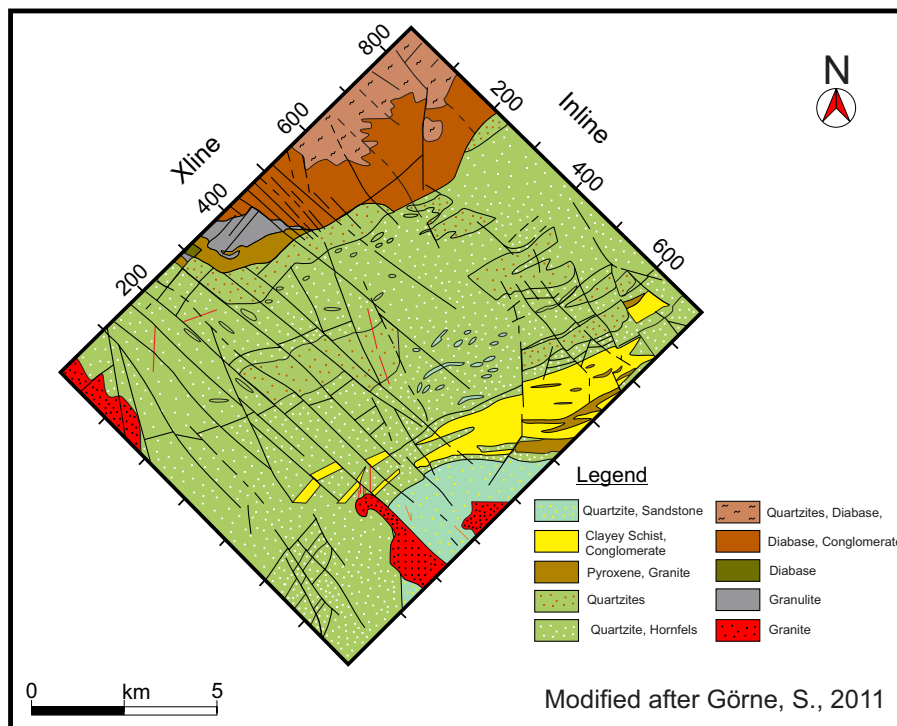


Figure 2: Geological map of the study area with in-line/cross-line coordinates.

Although a velocity analysis performed by a skilled processing specialist might help to improve the image quality of the CMP stack we wanted to explore the performance of the CRS method on hard rock data and applied it to aim for an improved S/N ratio and image quality. In Figure 4b the CRS stack of

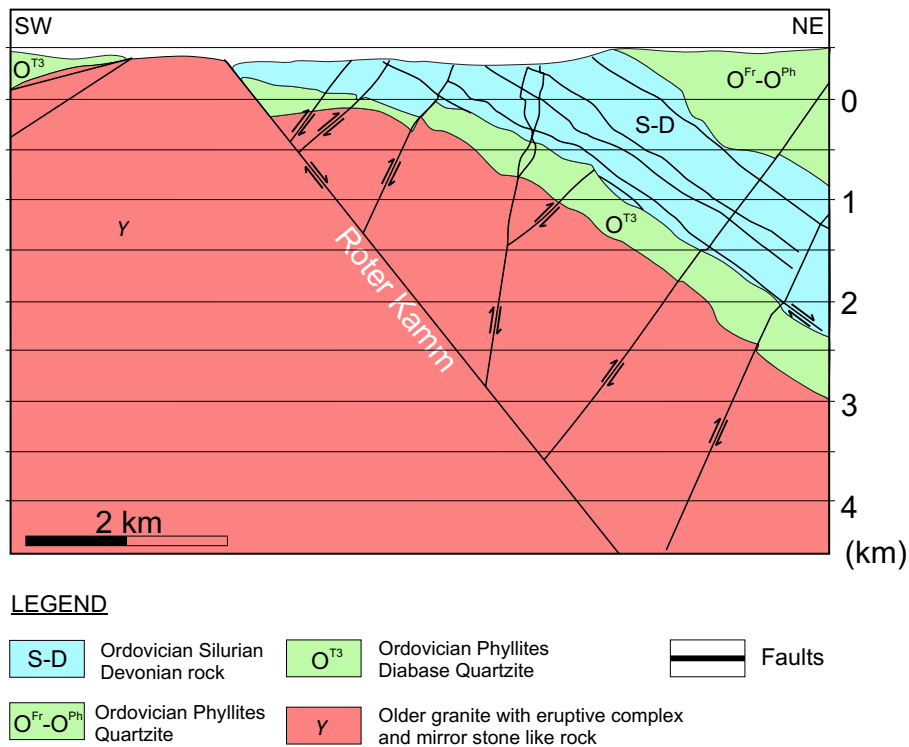


Figure 3: Geological cross section of the study area following approximately in-line 550

the same line is shown. Reflection events here are clearer, more continuous and more easy to distinguish in comparison to the CMP stack. Please note, that the color amplitude scales are different for both plots since the CRS stack has higher amplitudes and dynamic range than the amplitudes of the CMP stack. Although the quality of the CRS stacked section is already satisfactory because of the increased S/N we also considered the coherence as an imaging attribute since it is obtained in an objective data driven way during the optimization procedure.

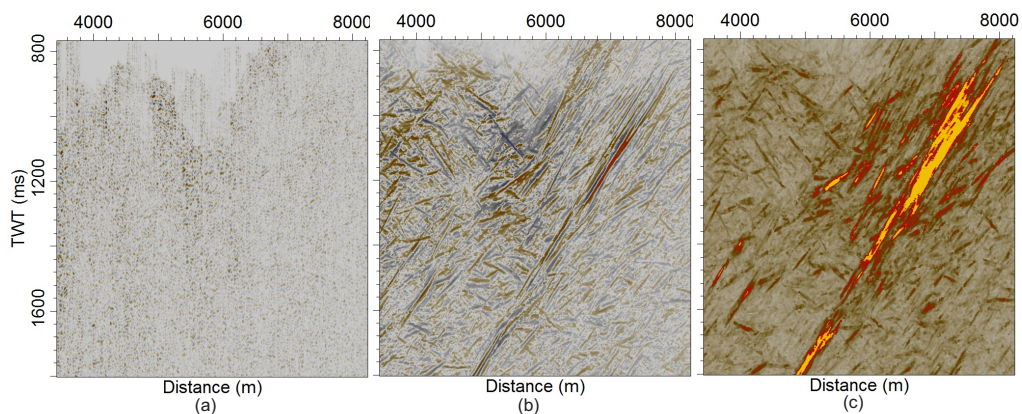


Figure 4: (a) CMP Stack, (b) CRS stack, (c) coherence of cross-line 600.

The coherence represents a low-pass positive definite version of the ZO stack image. It should display very similar features as the stack but with a decreased resolution. The coherence image of cross-line 600 is shown in Figure 4c. Please note again, that the color scale is different from the CMP and CRS sections in this figure since the coherence is always positive and assumes values between 0 and 1. For data with a very

good S/N ratio the coherence section should be similar to a stacked section where absolute amplitudes are considered. For noisy data, however, the coherence section is the superior choice since seismic noise does not stack destructively if absolute amplitudes are used. The coherence value directly reflects the physical relevance of the stack. In the coherence section it is obvious that the steep dipping continuous events crossing the whole section are of higher relevance than the events in the top left corner. This conclusion is not so easily derived from the CRS stacked section (Figure 4c). Therefore we decided that the coherence is the most suitable imaging attribute for the structural interpretation of this particular set of hard rock data.

In Figure 5 we show the post-stack time-migrated coherence section of in-line 290 which was obtained by a Kirchhoff method. A constant time migration velocity of 6.0 km/s was used since this velocity represents best the average properties of the area. A series of steeply dipping events with strong coherence is recognized. The events are caused by the series of conjugate faults as predicted by the geological surface data (see also Figure 3). The Roter Kamm does not display similarly as the conjugate faults. Some indications might be identified but the coherence of these events is considerably smaller and of very little lateral continuity than for the events attributed to the conjugate faults. The strong event in the right part of the section at about 1400 ms TWT is the reflection from the top of granite. Some stronger almost horizontal events are visible in the left part of the section at about 2200 ms. These events might be attributed to the transition to the lower crust. This interpretation, however, is still under discussion.

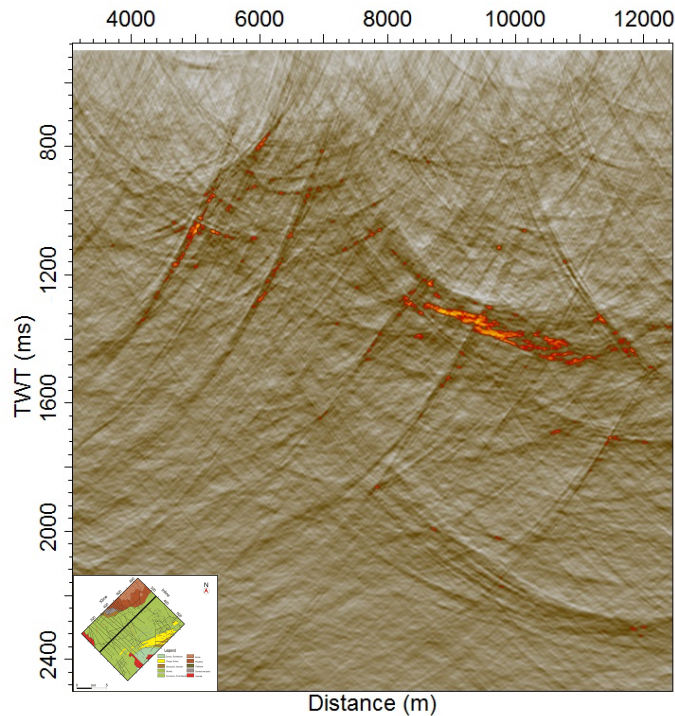


Figure 5: Time-migrated coherence section of in-line 290.

Figure 6 displays a migrated coherence time slice at 1330 TWT. The top and bottom reflections from the clayey schists represent the most prominent features of the time slice as well as the strong events in the mining area at the top corner of the image. A series of events of lower but still visible coherence is attributed to the sequence of conjugate faults. The coherence of these events increases with increasing cross-line numbers. The maximum lateral extend of the events is limited to in-lines 200-400. In the geological map of Figure 2 these faults have a much larger lateral extend on the surface and cut through the entire area. Again, no obvious evidence of the Roter Kamm is visible in this time slice.

A 3D cut through the time-migrated coherence volume is shown in Figure 7. The vertical surfaces correspond to in-line 130 and cross-line 600. The time slice is located at 2110 ms. Again the most prominent feature in this 3D image are the reflections from top and bottom of the clayey schists best visible in the

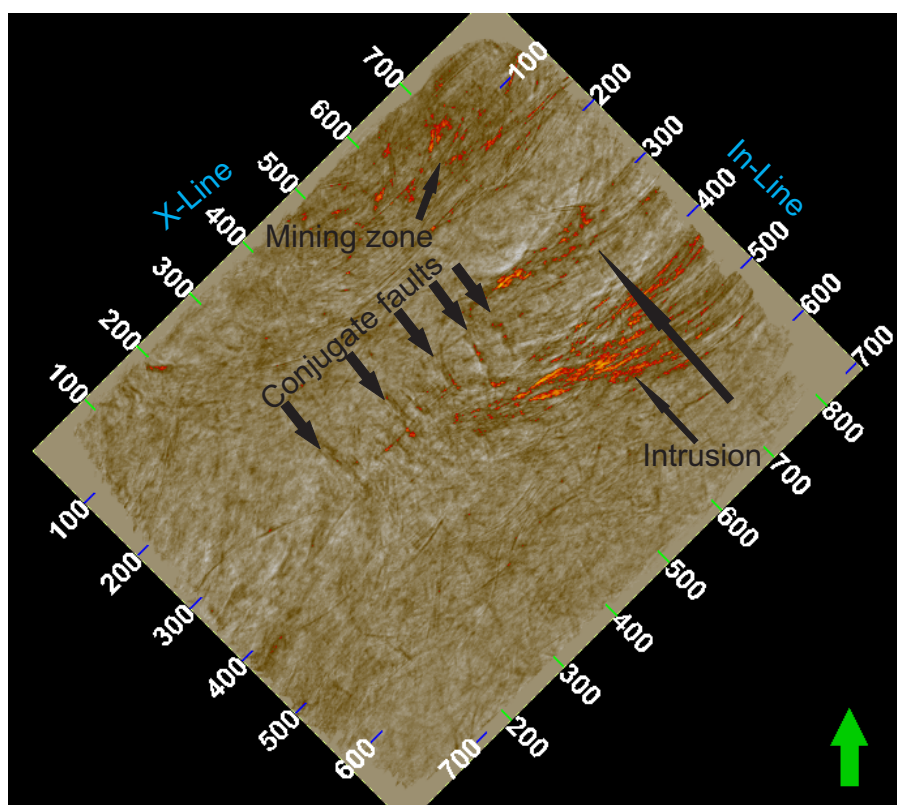


Figure 6: Time-migrated coherence time-slice at 1330 ms.

cross-line plot. Also the area with mining activity is clearly visible in the in-line section around cross-line 500. The event with strongest coherence at about 1000 ms represents the top of granite. No clear evidence of the Roter Kamm and only some low coherence events in the in-line section cutting the surface at about cross-line 220 and 300 can be attributed to the conjugate faults. We already saw in the time slice of Figure 6 that the lateral extent of the conjugate faults does not cross through the entire area. The 2110 ms time slice shows events of increased coherence in the area of cross-line 250 to 450 and in-line 100 to 300. In this region several fracture systems intersect and may lead to a highly fractured subsurface generating numerous diffraction events which are focused in the migrated section. This concentration of coherent energy in this area is even better visible in a 3D plot of the time migrated coherence displayed in transparency mode.

The 3D cube of Figure 8 represents another view of the data cube. Next to the top and bottom reflections from the clayey schists we observe an area of high coherence. The bottom of this zone corresponds to the events described above in the time-slice at 2110 ms. The coherence increases for smaller two-way times and covers a vertical section of about 1000 ms. The interpretation of these events is the same as above. In this region several fracture systems intersect and the fracture density is very high. These fractures generate diffractions which focus in the time migration. The apexes of the corresponding focused diffractions align to coherent events in some cases. From the current state of processing and interpretation we can not say, whether these fractures are open or mineralized. In case of open fractures these region could form a good target for geothermal heat exchange.

CONCLUSION

We have presented the application of the 3D CRS-based workflow to the Schneeberg 3D hard rock reflection seismic data. The S/N ratio of these data is very low and the CMP-stack did not provide good images suitable for interpretation. The data are dominated by diffractions generated at various steep dipping frac-

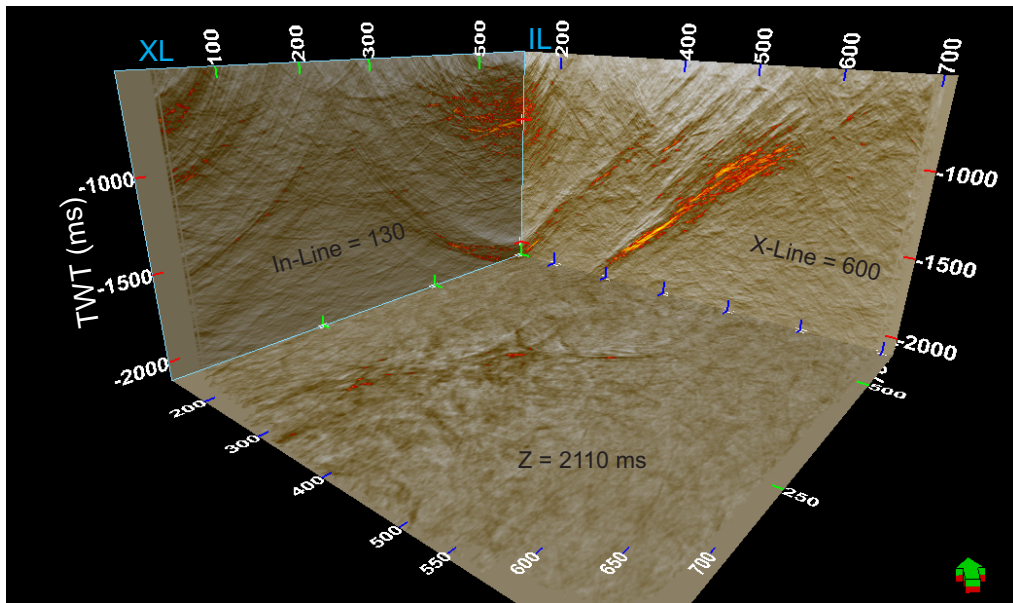


Figure 7: Time-migrated coherence volume at in-line 130, cross-line 600 and time-slice 2110 ms.

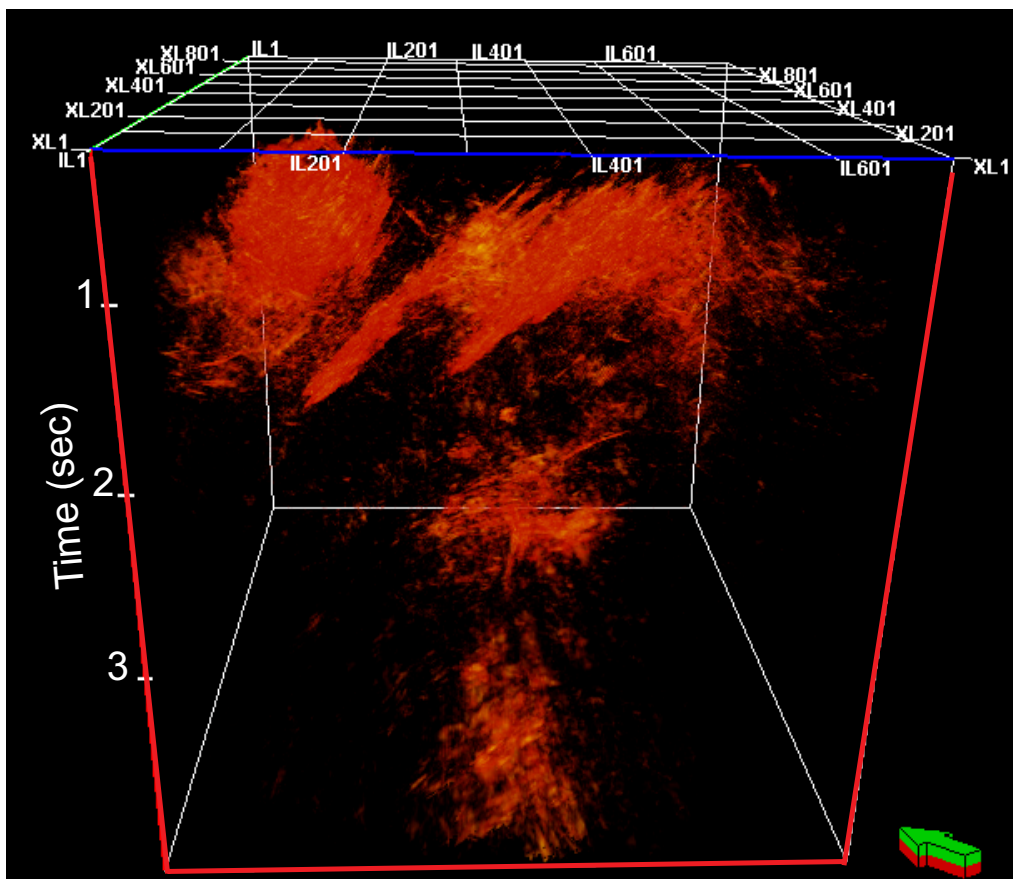


Figure 8: 3D time-migrated coherence cube displayed in transparency mode.

ture zones. Steep structures and a huge number of diffraction tails interfere or lead to a complicated pattern of conflicting dips. This makes the interpretation of the stacks very difficult. The CRS stack showed a considerably improved S/N ratio and provided a reasonable basis for geological interpretation. Plots of the coherence actually provided the best images for interpretation for this particular type of hard rock data. The coherence is an objective measure and directly reflects the physical relevance of the corresponding seismic event. We consider the coherence as an entirely data driven imaging attribute particularly helpful for the interpretation of hard rock data. Similar conclusions apply to the display of time slices where coherence slices provided the best images when compared to time slices out of the stacked volume. The presence of large diffraction events in the data requires migration for the interpretation of the sections. We applied post-stack Kirchhoff time migration making use of a constant velocity assumption. The obtained sections of the migrated volume show the major geological features of the area.

The reflections from top and bottom of clayey schists represent the most prominent feature in the data. We could also nicely map a sequence of conjugate faults. Their lateral extent at depth seems to be small which does not coincide with the surface expression of these faults. Prior to this experiment the Roter Kamm was expected to be the most prominent structure in the data. There are only faint hints of this fault in the data and the coherence is much smaller than the coherence of the sequence of conjugate faults. Another prominent feature of the data was best imaged in the time migrated 3D coherence cube using a transparency mode. This feature represents an area with a very high number of focused diffractions which partially even align to fractures. This area of high coherence is located at a region where several fracture systems intersect and may have a high fracture density. Whether these fractures are open or mineralized can not be decided from the current state of processing. Open fractures would make this area a favorable region for a geothermal heat exchanger. It is known, however, that many fracture systems in the North of the measurement surface are mineralized which initiated the mining activities in this area.

OUTLOOK

Pre-stack time and depth migration of hard rock data will rely on the quality of the underlying velocities for these processes. Because of the poor data quality the estimation of CRS attributes is not necessarily stable and all processes relying on these attributes may be compromised. This includes the determination of time migration velocities. Key element in the successful processing of hard rock data is the enhancement of the pre-stack data quality. Partial CRS stacks (Baykulov and Gajewski, 2009) might be the an option to improve the image quality. However, if the determined CRS stacking attributes are poor, the data enhancement result might not be effective. The data are largely dominated by diffractions which are not optimally fitted by the CRS operator. Processing the data with the i-CRS operator (Schwarz et al., 2014) might improve the determination of wave field attributes since it better fits diffractions. High quality attributes will result in better time migration velocities, improved NIP wave tomography and better pre-stack data enhancement opportunities. Another option of pre-stack data improvement is given by the partial time migration introduced by Dell et al. (2012). This tool also has a pre-stack data enhancement facility and requires reasonable time migration velocities to be applied effectively.

ACKNOWLEDGMENTS

Special thanks go to the BMU (Bundesministerium für Umwelt, Naturschutz und Reaktorsicherheit), German Ministry of Science and Technology for funding the field work and the processing. The discussions with the project partners of the University of Freiberg, Freiberg, Germany and, Leibniz Institute for Applied Geophysics, Hannover, Germany, are highly appreciated. We would like to thank the Applied Geophysics Group Hamburg for continuous discussions. This work was also partially supported by the sponsors of the *Wave Inversion Technology (WIT) Consortium*. Dela Spickermann, Michael Böttinger and Hendryk Bockelmann from DKRZ (Deutsches Klimarechenzentrum) greatly helped to meet computational demands.

PS: This report has been submitted for publication in Geophysical Prospecting (Special issue for hardrock seismic imaging) and is under the review process now.

REFERENCES

- Baykulov, M., Dümmong, S., and Gajewski, D. (2011). From time to depth with CRS attributes. *Geophysics*, 76(4):S151–S155.
- Baykulov, M. and Gajewski, D. (2009). Prestack seismic data enhancement with partial common-reflection-surface (CRS) stack. *Geophysics*, 74(3):V49–V58.
- Bergler, S., Hubral, P., Marchetti, P., Cristini, A., and Cardone, G. (2002). 3D common-reflection-surface stack and kinematic wavefield attributes. *The Leading Edge*, 21(10):1010–1015.
- Dell, S. and Gajewski, D. (2011). Common-reflection-surface-based workflow for diffraction imaging. *Geophysics*, 76(5):S187–S195.
- Dell, S., Gajewski, D., and Vanelle, C. (2012). Prestack time migration by common-migrated-reflector-element stacking. *Geophysics*, 77(3):S73–S82.
- Dümmong, S. and Gajewski, D. (2008). A multiple suppression method via CRS attributes. *2008 SEG Expanded Abstracts*, pages 2531–2535.
- Duveneck, E. (2004). Velocity model estimation with data-derived wavefront attributes. *Geophysics*, 69(1):265–274.
- Emmermann, R. and Wohlenberg, J. (1988). *German Continental Deep Drilling Program (KTB)*. Springer.
- Hertweck, T., Schleicher, J., and Mann, J. (2007). Data stacking beyond CMP. *The Leading Edge*, 26:818–827.
- Hubral, P. (1983). Computing true amplitude reflections in a laterally inhomogeneous earth. *Geophysics*, 48(8):1051–1062.
- Malehmir, A., Durrheim, R., Bellefleur, G., Urosevic, M., Juhlin, C., White, D. J., Milkereit, B., and Campbell, G. (2012). Seismic methods in mineral exploration and mine planning: A general overview of past and present case histories and a look into the future. *Geophysics*, 77(5):WC173–WC190.
- Mann, J., Jäger, R., Müller, T., and Hubral, P. (1999). Common-reflection-surface-stack - a real data example. *J. Appl. Geoph.*, 42(3,4):283–300.
- Milkereit, B., Berrer, E., King, A. R., Watts, A. H., Roberts, B., Adam, E., Eaton, D. W., Wu, J., and Salisbury, M. H. (2000). Development of 3-D seismic exploration technology for deep nickel-copper deposits-A case history from the Sudbury basin, Canada. *Geophysics*, 65(6):1890–1899.
- Müller, N.-A. (2003). The 3D Common-Reflection-Surface stack – Theory and application. Master's thesis, University of Karlsruhe.
- Schwarz, B., Vanelle, C., Gajewski, D., and Kashtan, B. (2014). Curvatures and inhomogeneities: An improved common-reflection-surface approach. *Geophysics*, 79(5):S231–S240.